Editors' Suggestion

Deterministic Switching of Polarization Vortices in Compositionally Graded Ferroelectrics Using a Mechanical Field

Le Van Lich,[1,*] Tinh Quoc Bui,[2] Takahiro Shimada,[3] Takayuki Kitamura,[3] Trong-Giang Nguyen,[1] and Van-Hai Dinh[1]

[1] *School of Materials Science and Technology, Hanoi University of Science and Technology, No. 1 Dai Co Viet Street, Hanoi, Vietnam*

[2] *Department of Civil and Environmental Engineering, Tokyo Institute of Technology, 2-12-1-W8-22, Ookayama, Meguro-ku, Tokyo 152-8552, Japan*

[3] *Department of Mechanical Engineering and Science, Kyoto University, Nishikyo-ku, Kyoto, 615-8540, Japan*

(Received 3 February 2019; revised manuscript received 2 April 2019; published 1 May 2019)

Deterministic switching of polarization vortices in ferroelectrics by a uniaxial mechanical load is challenging. Here, we demonstrate, by using phase field simulations and ferroelectric instability analyses, a deterministic switching of polarization vortices in a compositionally graded ferroelectric (CGFE) nanoplate under a compressive stress. The obtained results suggest that the rational distribution of material constituents in the CGFE nanoplate tailors the distributions of electromechanical coupling and total energy densities of the nanoplate, which modifies the stress-induced vortex multiplication and annihilation behaviors, distinguished from those in a homogeneous ferroelectric nanoplate. The switching of polarization vortices by compressive stress is verified through instability analyses for the CGFE nanoplate, which not only confirms when the polarization switching occurs, but also demonstrates how the polarization responds at the onset of the switching. In addition, the effects of various factors on the feasibility of stress-induced vortex switching, including material gradient, temperature, and width-to-height ratio of the CGFE nanoplate, are investigated and summarized in phase diagrams.

DOI: 10.1103/PhysRevApplied.11.054001

I. INTRODUCTION

A ferroelectric vortex is a swirling polarization configuration around a stable central core, which is characterized by its vorticity of in-plane polarization vectors, i.e., clockwise (CW) and counterclockwise (CCW) rotations [1]. Although polarization vortex structure was predicted decades ago [1–6], experimental observations of the polarization vortex have been achieved only in recent years [7–10]. The realization of the polarization vortex opens exciting opportunities for alternative ferroelectric-based nanodevices. For instance, the bistability of CW and CCW vortices is appealing for nonvolatile memory storage concepts [1]. Moreover, the properties of electronic transport at the vortex core are quite promising for the design and implementation of integrated oxide electronic devices based on vortex domain structures [11]. For a reliable implementation of vortices in such applications, the prerequisite is an effective control of the polarization vortex, i.e., deterministic switching of the polarization vortex.

Controlling polarization vortices has attracted great attention over the past decade. An early idea is to utilize a curled electric field to switch the polarization vortex [12–14]. However, the magnitude of the applied field that is necessary for the switching of electric toroidal moment is difficult to generate in practice [15]. Alternatively, a homogeneous electric field has been proposed to switch the polarization vortex in ferroelectric systems with rational designs of nanostructures, such as asymmetric ferroelectric nanorings [16], dot-film systems [17], and asymmetric ferroelectric nanodisks [18]. Another attempt has been made to switch the polarization vortex using a homogeneous electric field with the mediation of asymmetric mechanical fields caused by substrate, dislocations, and local clamping force [19].

Investigations on the switching of polarization vortices have been mostly focused on electrical switching, where the electrostatic interaction between polarization and the external electric field is exploited to control the switching behavior. However, the ferroelectric aging and fatigue phenomena are common issues emerging in the electrical switching [20–23]. Other than the electrostatic interaction, ferroelectric materials intrinsically include the electromechanical coupling between polarization and strain (or stress), which makes ferroelectrics susceptible to a mechanical excitation. Since the electromechanical coupling is distinct from the electrostatic interaction, it is

*levanlichbk@gmail.com

expected that the mechanical switching of a polarization vortex (if possible) should follow a different pathway from that of electrical switching. On the other hand, the vortex switching process generally proceeds through a nucleation of a new vortex with opposite vorticity, followed by the annihilation of the initial vortex [12,13]. In addition, the nucleation and annihilation of vortices can be induced by both electric fields and mechanical fields [24–26]. This result indicates a possibility of vortex switching via mechanical fields. Pursuing the mechanical switching of polarization vortices, a recent study [27] showed that, by introducing a physical pore in a ferroelectric nanoplate, a closure flux polarization pattern can be switched by mechanical load. However, such a porous nanoplate inevitably excludes the physical vortex core in the closure-flux pattern, which is topologically distinguished from a polarization vortex [28–30]. Since the characterized properties of polarization vortices mostly exhibit at the vortex core and its vicinity region [11,31,32], the appearance of a physical pore significantly degrades or even eliminates the vortex properties. In addition, the presence of a pore in a nanoplate brings about a high stress concentration near the pore under mechanical load [27], giving rise to a serious concern in the fracture resistance of the porous nanoplate due to the inherent brittleness and low fracture toughness of ferroelectrics [33,34]. Therefore, the deterministic switching of a polarization vortex by mechanical loads remains elusive, in spite of its strong possibility. More recently, an electromechanical control of polarization vortex ordering has been investigated in a system of two interacting ferroelectric nanoparticles surrounded by an elastic medium [35]. The obtained results suggested that by applying an electric field, a mechanical strain is transferred into the elastic matrix and facilitates preferential switching of the vortexlike patterns.

In general, the switching of polarization vortices is governed by the nucleation and annihilation process of polarization vortices; thus, if one can control the trajectory of this process, the switching of polarization vortex can be achieved. Recent significant advances in manufacturing technology have enabled us to obtain compositionally graded ferroelectric (CGFE) heterostructures [36,37]. In CGFE nanostructures, the material compositions are site dependent, which gives rise to gradients in both polarization and strain fields. The intrinsic polarization and strain gradients significantly modify the electromechanical coupling interaction in CGFE nanostructures in comparison to that in the homogeneous ferroelectric (HFE) counterparts [37]. Since the nucleation and annihilation process of a vortex under mechanical fields is dominated by the electromechanical coupling interaction, such a modification of the electromechanical coupling interaction in CGFEs is quite promising to exploit for a control of the vortex nucleation and annihilation process and, therefore, has potential for the feasibility of vortex switching in CGFE by mechanical fields.

In this paper, we conduct phase field simulations and ferroelectric instability analyses to demonstrate a deterministic switching of the polarization vortex in a CGFE nanoplate under a compressive stress. The material constituents are assumed to linearly vary in the long axis direction of the nanoplate. The compositional gradient of materials strongly affects the stress-induced vortex multiplication and annihilation behaviors in the CGFE nanoplate. Consequently, a deterministic switching of a polarization vortex can be realized after a stress loading and unloading process. In addition, we systematically discuss the effects of material gradient, temperature, and shape of the CGFE nanoplate on the switching of a polarization vortex under stress.

II. METHODS

A. Phase field model for compositionally graded ferroelectrics

The formation and switching of domain structures in CGFE nanoplates under a mechanical field are investigated using the phase field model based on the Ginzburg-Landau theory. In this study, we modify the phase field model of HFEs [18,38–42] and then apply it for CGFEs by including the site-dependent character into the model. As a typical example, CGFE material is selected as $Pb_{1-x}Sr_xTiO_3$ (PST), where the material parameters are assumed to be a weighted linear average of the constituent materials [43,44], i.e., $PbTiO_3$ (PT) and $SrTiO_3$ (ST), as

$$\xi^x = (1-x)\xi^{\mathrm{PT}} + x\xi^{\mathrm{ST}}, \tag{1}$$

where ξ^x are any material parameters, such as the dielectric stiffness, elastic constants, electrostrictive constants, and Curie temperature of constitution materials, corresponding to a particular mole fraction, x, of ST in PST material; ξ^{PT} and ξ^{ST} are any given material parameters for pure PT and ST, respectively.

To easily compare and see the distinction between phase field models of HFEs and CGFEs, we present the phase field model of CGFEs in a similar manner with that of HFEs described in a previous study [18]. In addition, energy components of the CGFE system, which include varying material parameters according to material constituents, are marked with superscript x. In the phase field model of CGFEs, three physical fields, including the displacement $\mathbf{u}(=u_i)$, electric potential ϕ, and polarization $\mathbf{p}(=p_i)$, are required to describe behaviors of the materials, in which the spontaneous polarization vector is usually regarded as the material order parameter. Therefore, the electrical enthalpy f_{FE}^x is a function of polarization p_i, polarization gradient $\nabla_i p_j$, electric field E_i, and strain ε_{ij}, where $\nabla_i p_j = \partial p_j/\partial x_i$, $E_i = \partial\phi/\partial x_i$, and $\varepsilon_{ij} = (\partial u_i/\partial x_j +$

$\partial u_j/\partial x_i)/2$ $(i,j = 1, 2, 3)$. The electrical enthalpy f_{FE}^x is given by

$$f_{\mathrm{FE}}^x = f_L^x(p_i) + f_G^x(\nabla_i p_j) + f_{\mathrm{Elas}}^x(\varepsilon_{ij}) + f_{\mathrm{Coup}}^x(\varepsilon_{ij}, p_i) + f_E^x(p_i, E_i), \tag{2}$$

where $f_L^x(p_i)$, $f_G^x(\nabla_i p_j)$, $f_{\mathrm{Elas}}^x(\varepsilon_{ij})$, $f_{\mathrm{Coup}}^x(\varepsilon_{ij}, p_i)$, and $f_E^x(p_i, E_i)$ denote the Landau, gradient, elastic, electromechanical coupling, and electrostatic energy densities, respectively. Detailed expressions of these energy densities are presented in similar forms to those in previous studies [18,45]. The total energy of the CGFE system Π is obtained by integrating the electrical enthalpy over the entire volume of the CGFE system V, implying

$$\Pi = \int_V \left[\int_x f_{\mathrm{FE}}^x dx \right] dV. \tag{3}$$

The temporal evolution of the polarization field toward its thermodynamic equilibrium state is governed by the time-dependent Ginzburg-Landau (TDGL) equation, as follows:

$$\frac{\partial p_i(r,t)}{\partial t} = -\mathcal{L}\frac{\delta \Pi}{\delta p_i(r,t)}, \tag{4}$$

where t denotes evolution time, $r = (x_1, x_2, x_1)$ is the spatial vector, and $\mathcal{L}$ is a kinetic coefficient. In addition to the TDGL equation, the mechanical equilibrium and Maxwell (or Gauss) equations must be satisfied simultaneously with respect to body force-free and charge-free CGFE materials as follows:

$$\frac{\partial}{\partial x_j}\left(\frac{\partial f_{\mathrm{FE}}^x}{\partial \varepsilon_{ij}}\right) = 0 \tag{5}$$

and

$$\frac{\partial}{\partial x_i}\left(-\frac{\partial f_{\mathrm{FE}}^x}{\partial E_i}\right) = 0. \tag{6}$$

To solve these equilibrium equations [Eqs. (4)–(6)], a numerical algorithm based on the finite-element method (FEM) is employed in the present study. For the space discretization, hexahedral elements with seven degrees of freedom (DOFs) at each node, i.e., u_i, ϕ, p_i, are taken. All the governing equations are solved in real space. The implementation of the phase field model of CGFE in a FEM framework is described in detail in the previous study [46].

B. Instability analysis for ferroelectrics

We consider a three-dimensional finite-element model of a continuum ferroelectric system consisting of N nodes. The potential energy of the system U can be described as

$$U = U(\mathbf{u}, \phi, \mathbf{p}), \tag{7}$$

where

$$\mathbf{u} = (u_1^1, u_2^1, u_3^1, u_1^2, u_2^2, u_3^2, \ldots, u_1^N, u_2^N, u_3^N)^T, \tag{8}$$

$$\phi = (\phi^1, \phi^2, \ldots, \phi^N)^T, \tag{9}$$

$$\mathbf{p} = (p_1^1, p_2^1, p_3^1, p_1^2, p_2^2, p_3^2, \ldots, p_1^N, p_2^N, p_3^N)^T. \tag{10}$$

Here, u_i^α, ϕ^α, and p_i^α respectively represent the displacement, electrical potential, and polarization vector at the node αth in the x_i direction. According to the previous study [14], the irreducible number of DOFs in the considering system is $7N - 7$. For simplicity, all irreducible DOFs of the system are represented by the following m-dimensional vector d:

$$\begin{aligned} d = (&u_3^2, u_1^3, u_2^3, u_1^4, u_2^4, u_3^4, \ldots, u_1^N, u_2^N, u_3^N, \phi^2, \phi^3, \ldots, \phi^N, \\ &p_1^1, p_2^1, p_3^1, p_1^2, p_2^2, p_3^2, \ldots, p_1^N, p_2^N, p_3^N)^T \\ = &(d_1, d_2, \ldots, d_m)^T. \end{aligned} \tag{11}$$

When the system is in a thermodynamic equilibrium state $(d = d_0)$, the polarization vectors are unchanged under a static mechanical load. Generally, the total energy of the system Π consists of the potential energy U and the work done by an external mechanical load W. It is given by

$$\Pi = U + W. \tag{12}$$

The total energy of the system in terms of an infinitesimal deformation and/or perturbation of the polarization vector, $\Pi(d_0 + \Delta d)$, can be described by the Taylor series expansion of the total energy, $\Pi(d_0)$, with Δd, and is described as

$$\Pi(d_0 + \Delta d) = \Pi(d_0) + \sum_{k=1}^{m} \left.\frac{\partial \Pi}{\partial d_k}\right|_{d=d_0} \Delta d_k + \frac{1}{2}\sum_{k=1}^{m}\sum_{l=1}^{m} \left.\frac{\partial^2 \Pi}{\partial d_k \partial d_l}\right|_{d=d_0} \Delta d_k \Delta d_l + \cdots \tag{13}$$

At the thermodynamic equilibrium state, the stability condition requires minimization of the total energy. In the other words, the second term on the right-hand side (the first derivative of total energy) in Eq. (13) must be zero

[14,47–50], i.e.,

$$\sum_{k=1}^{m} \left.\frac{\partial \Pi}{\partial d_k}\right|_{d=d_0} \Delta d_k = 0. \tag{14}$$

In addition, the external load is constant due to the static loading; therefore,

$$\left.\frac{\partial^2 W}{\partial d_k \partial d_l}\right|_{d=d_0} = 0. \tag{15}$$

By ignoring the higher-order terms, the change in total energy $\Delta\Pi$ can be rewritten as

$$\Delta\Pi = \Pi(d_0 + \Delta d) - \Pi(d_0) = \tfrac{1}{2}\Delta d^T H \Delta d, \tag{16}$$

where H is the $m \times m$ Hessian matrix. The components of the Hessian matrix are given by the second derivative of the total energy with respect to the DOFs as follows:

$$H_{kl} = \left.\frac{\partial^2 \Pi}{\partial d_k \partial d_l}\right|_{d=d_0} = \left.\frac{\partial^2 U}{\partial d_k \partial d_l}\right|_{d=d_0}. \tag{17}$$

The eigenvalues η_i ($\eta_1 \leq \cdots \leq \eta_i \leq \cdots \leq \eta_m$) and the corresponding eigenvectors ν_i of matrix H are obtained by solving the following eigenvalue problem:

$$H\nu_i = \eta_i \nu_i. \tag{18}$$

Using the eigenvectors ν_i, the matrix H is diagonalized as

$$V^{-1}HV = V^T HV = \begin{bmatrix} \eta_1 & & 0 \\ & \ddots & \\ 0 & & \eta_m \end{bmatrix}, \tag{19}$$

where $V = (\nu_1, \nu_2, \ldots, \nu_m)$. Introducing

$$\Delta Q = V^{-1}\Delta d = (\Delta Q_1, \ldots, \Delta Q_m)^T, \tag{20}$$

the total energy change in Eq. (16) becomes

$$\begin{aligned} \Delta\Pi &= \frac{1}{2}(V\Delta Q)^T H (V\Delta Q) = \frac{1}{2}\Delta Q^T \left(V^T H V\right)\Delta Q \\ &= \frac{1}{2}\sum_{i=1}^{m} \eta_i (\Delta Q)^2. \end{aligned} \tag{21}$$

A previous study [14] indicated that the critical condition for instability ($\Delta\Pi = 0$) appears when the minimum eigenvalue reaches zero ($\eta_1 = 0$) and the corresponding eigenvector ν_1 at $\eta_1 = 0$ represents the change in the polarization vector and the elastic deformation at the instability, i.e., the instability mode vector.

C. Simulation models and procedure

In the present study, we focus on nanoplates made of CGFEs, in which the constituent materials vary linearly as $Pb_{0.8}Sr_{0.2}TiO_3$(Top)⇔$PbTiO_3$(Middle)⇔$Pb_{0.8}Sr_{0.2}TiO_3$ (Bottom) (namely, PST20⇔PT⇔PST20), as shown in Fig. 1. For comparison, a nanoplate with the same size, yet made of HFE $Pb_{0.9}Sr_{0.1}TiO_3$ (PST10) is also considered. Note that the averaged mole fractions of material constituents in CGFE and HFE nanoplates are selected the same. Figure 1 shows the geometries of nanoplates used in the present study. To intentionally form a spontaneous polarization vortex, the dimensions of nanoplates are set in a range from several to tens of nanometers, which takes into account the strong depolarization field at free surfaces of the nanoplates [1,51]. Therefore, the thickness of nanoplates t is prepared at 10 nm, while the width w and height h are set to be 16 and 24 nm, respectively. Three-dimensional (3D) discrete grids with brick elements are employed. The size of the smallest element is less than 0.4 nm. A default simulated temperature is set to be near room temperature (300 K), unless otherwise specified when the temperature effect is discussed. Values of all material parameters used in this work for pure PT and pure ST materials are listed in previous studies [26,52,53].

In order for ferroelectric nanoplates to attain thermodynamic equilibrium without external fields, a random distribution of polarization with infinitesimal magnitude is introduced into the systems as an initial condition and the evolution of the polarization field is numerically simulated by iteratively solving the TDGL equation. A backward Euler scheme and Newton iteration method are integrated into the FEM algorithm for the time integration and nonlinear iteration, respectively. The polarization configuration is stably formed when the change of total energy magnitude in the considered system is below 10^{-3} eV. Previous studies suggested that a compression can trigger the nucleation of new vortices. Therefore, in this study, a uniform compressive stress σ_{app} is applied in a step-wise manner

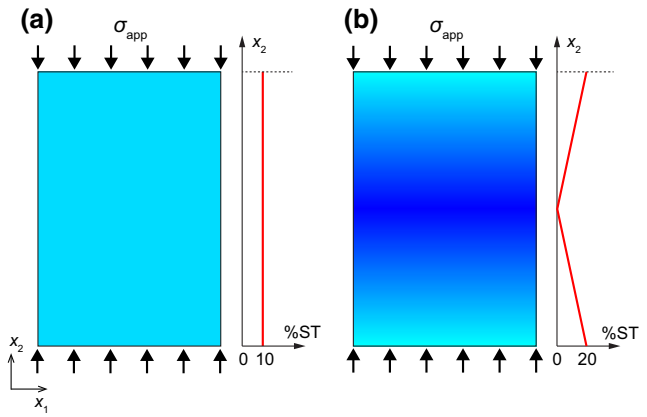

FIG. 1. Geometries and loading conditions of (a) HFE and (b) CGFE nanoplates.

to the nanoplates along the x_2 direction with periodic triangular waves to investigate the polarization switching behaviors. At each value of σ_{app}, the computational time is set to be sufficiently long, in order for the ferroelectric system to reach an equilibrium domain structure. The maximum value of compressive stress is set to be sufficiently high to ensure that saturation of the polarization switching could be reached.

III. RESULTS AND DISCUSSIONS

A. Spontaneous polarization pattern of ferroelectric nanoplates

Figures 2(a) and 2(b) depict the equilibrium distributions of polarization field and stresses in HFE and CGFE nanoplates, respectively. In both nanoplates, the spontaneous polarizations are arranged in a head-to-tail manner and form a single-vortex domain structure [1]. Figures 2(a1) and 2(b1) show the CCW polarization vortices in HFE and CGFE nanoplates, respectively. The polarization vortex is characterized by toroidal moment of polarization G_3, which is defined as $G_3 = (1/V)\int_V (r_i \times p_i)dV$, where r_i is the position vector of polarization p_i and V is volume of the nanoplate. The direction of the toroidal moment vector is perpendicular to the vortex plane, which is along the x_3 direction in the present study. Magnitudes of toroidal moments are determined equal to 2.83 and 3.22 e/Å for the HFE and CGFE nanoplates, respectively. On the other hand, in the HFE nanoplate, the polarization magnitude is nearly uniform, except for the domain wall and vortex-core areas, as shown in Fig. 2(a2). However, in the CGFE nanoplate, the magnitudes of polarization vectors are high in the middle of the CGFE nanoplate and gradually decrease toward the top and bottom surfaces [Fig. 2(b2)]. The spatial gradation in polarization magnitude originates from the compositional gradient of ST in the CGFE nanoplate, which is consistent with experimental observation [37]. In addition, the polarization magnitudes at domain wall and vortex-core areas are relatively small in comparison to that in the remaining area. Moreover, distributions of stress components σ_{11} and σ_{22} in the two nanoplates suggest that the stresses highly concentrate near the vortex cores, which is also consistent with previous studies on HFEs [26,32,54]. Importantly, the stress gradients in the CGFE nanoplate become steeper than that in the homogeneous counterpart. Therefore, not only polarization but also stress fields in the CGFE nanoplate are altered in comparison to those in the HFE nanoplate,

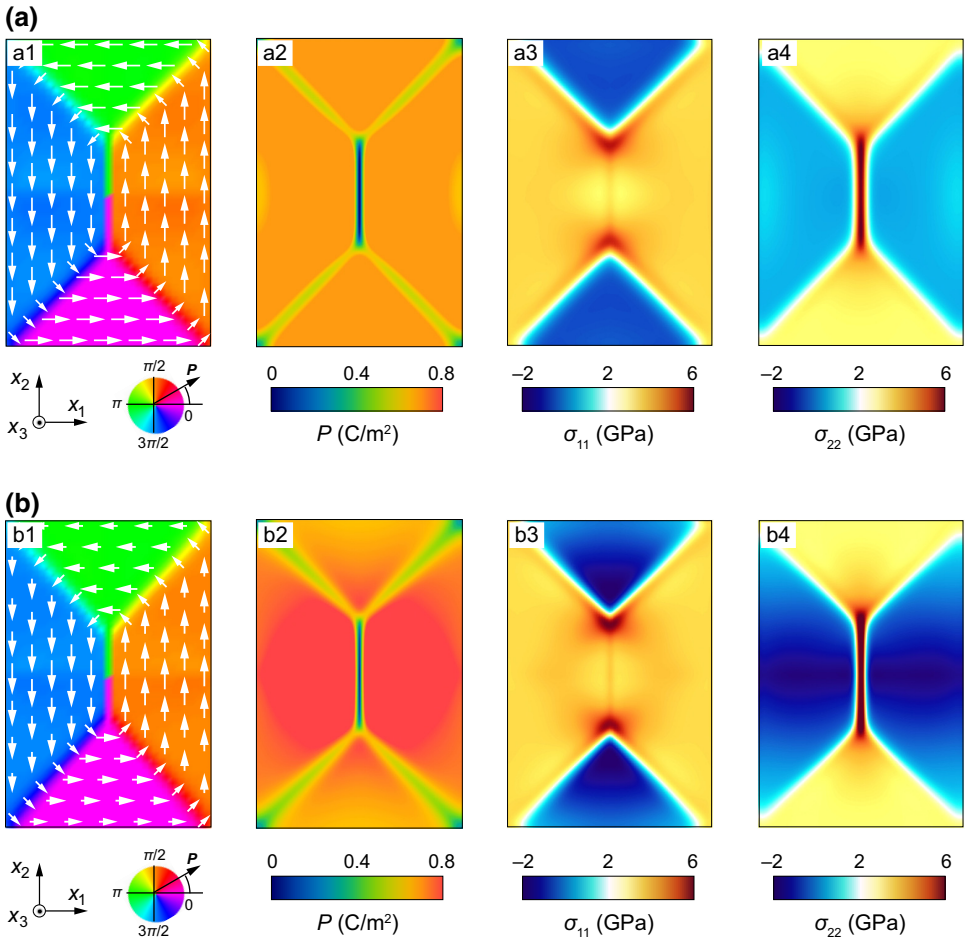

FIG. 2. Polarization vortex structures, distributions of polarization magnitude, stresses, and total energy densities in (a) HFE and (b) CGFE nanoplates.

which originates from the partial distribution of material constituents in the CGFE nanoplate. Such distinctions may bring about a different electromechanical coupling in the CGFE nanoplate, and thereby, a different switching pathway under mechanical loads.

B. Stress-induced switching of polarization vortex in ferroelectric nanoplates

To gain more insight into the effect of the compositional gradient on the polarization vortex switching, we investigate the polarization evolution of the CGFE nanoplate under mechanical load in comparison with that in its homogeneous counterpart. The obtained results for a HFE nanoplate are firstly presented for clarity.

Figures 3(a) and 3(b) show the domain evolution in the HFE nanoplate under a triangular wave of compression. Figure 3(a) visualizes the toroidal moment G_3 as a function of σ_{app}. The evolution direction is marked by several typical points from $H1$ to $H5$. The corresponding polarization domain patterns from point $H1$ to point $H5$ are depicted in Fig. 3(b). The initial state polarization pattern is taken with the CCW single vortex, as shown at point $H1$

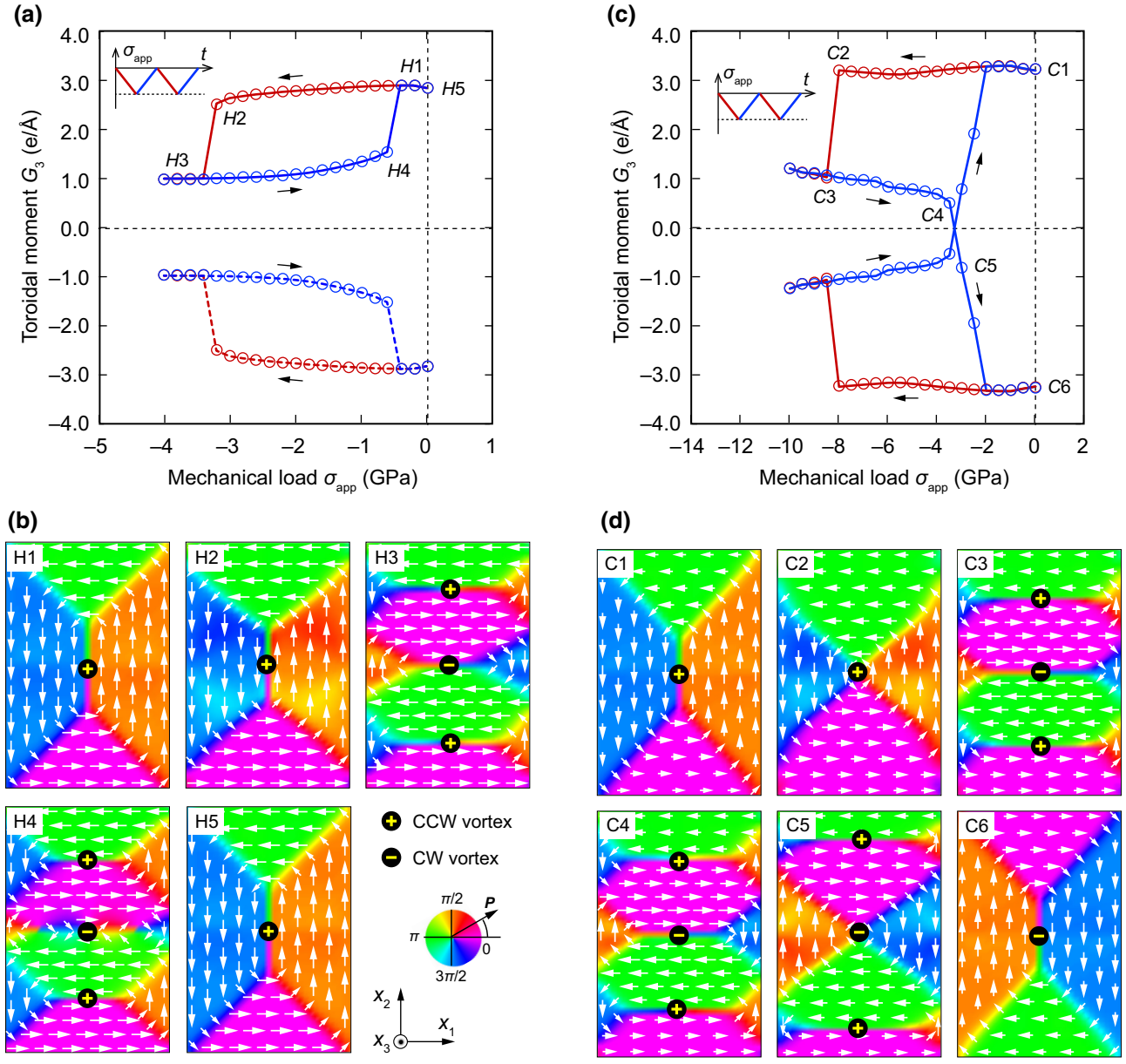

FIG. 3. (a) Toroidal moment of polarization vortex as a function of mechanical load in HFE nanoplate. The direction of the evolution is indicated by black arrows and marked by several points from $H1$ to $H5$. (b) The corresponding domain structures from point $H1$ to point $H5$. (c) Toroidal moment of polarization vortex as a function of mechanical load in CGFE nanoplate. The direction of the evolution is indicated by black arrows and marked by several points from $C1$ to $C6$. (d) The corresponding domain structures from point $C1$ to point $C6$.

in Fig. 3(b). At the first decrease process of the mechanical load from $H1$ to $H3$, as σ_{app} decreases from 0 to -4.0 GPa, the toroidal moment G_3 slightly decreases from 2.83 to 2.5 e/Å, then suddenly drops to 0.99 e/Å at $\sigma_{app} = -3.2$ GPa. An observation of the domain structures reveals that the initial single vortex evolves into triple vortices with alternative CCW-CW-CCW vorticities, which causes the drop in magnitude of the toroidal moment. In the increase process from $H3$ to $H5$, as σ_{app} increases from -4.0 to 0 GPa, the toroidal moment G_3 slightly increases and then abruptly jumps from 1.20 to 2.80 e/Å at $\sigma_{app} = -0.8$ GPa. The corresponding domain structures indicate a transformation from the triple-vortex state to the single-vortex state, in which two CCW vortices near the top and bottom surfaces expand to annihilate the middle CW vortex and then merge into a single vortex. Importantly, the newly formed single vortex has CCW vorticity, which is the same as that of the original single vortex. A similar tendency is observed for the vortex switching starting from a CW single vortex, as shown by the dashed lines in Fig. 3(a). Although Fig. 3(a) exhibits a mechanical hysteresis loop of toroidal moment where a transformation between single-vortex and triple-vortex states occurs, the rotation of polarization vectors in the single vortex cannot be reversed. This result is also consistent with the switching behaviors in HFEs with different averaged mole fractions of material constituents [24]. Therefore, the switching of a polarization vortex in a HFE nanoplate by compression is prohibited. In the following, the switching behavior similar to that in Figs. 3(a) and 3(b) is defined as type A.

Figures 3(c) and 3(d) show the domain evolution of a CGFE nanoplate under a triangular wave of compression. The initial polarization structure adopts a CCW single vortex, as depicted at point $C1$ in Fig. 3(d). At the first decrease process of the mechanical load from $C1$ to $C3$, as σ_{app} decreases from 0 to -10 GPa, the initial single vortex transforms into triple vortices, manifested with a sudden decrease of G_3 from 3.22 to 1.04 e/Å at $\sigma_{app} = -8.2$ GPa. The triple-vortex state has alternative CCW-CW-CCW vorticities. The domain evolution and the evolution paths during the first decrease process of the mechanical load in the CGFE nanoplate are similar to those in the HFE nanoplate shown in Figs. 3(a) and 3(b). However, the transformation from single- to triple-vortex states in a CGFE nanoplate occurs at a larger magnitude of stress, in comparison to that in the homogeneous counterpart. This result indicates that the single vortex in the CGFE nanoplate is more stable than that in the HFE nanoplate. In the increase process of the mechanical load from $C3$ to $C6$, as σ_{app} increases from -10 to 0 GPa, the toroidal moment gradually decreases. Then it decreases dramatically and achieves a negative value as σ_{app} is as large as -3.0 GPa. When σ_{app} completely releases, the toroidal moment achieves a high negative value of -3.22 e/Å. An observation of domain structure indicates that the middle CW vortex expands and clears away two CCW vortices near the top and bottom surfaces. Therefore, only one single vortex remains as the applied stress releases. Importantly, the remaining single vortex has CW vorticity, which is opposite to the initial CCW vorticity. In the subsequent period of mechanical loading, the CW single vortex can be switched back to the original CCW single vortex, such that the evolution path follows a reverse tendency in comparison to that in the previous period of mechanical loading. This result demonstrates a deterministic switching of a single vortex in the CGFE nanoplate. In Fig. 3(c), a butterfly loop characterizing the change of toroidal moment due to an applied compression is striking. The switching behavior similar to that in Figs. 3(c) and 3(d) is defined as type B.

C. Origin of stress-induced vortex switching in CGFE nanoplate

To validate stress-induced switching of polarization vortex in CGFE nanoplate, an investigation on the instability behavior of polarization is conducted. The instability criterion is determined by calculating the minimum eigenvalue of the Hessian matrix with a consideration of all degrees of freedom.

First of all, we consider the instability behavior of the domain structure in a HFE nanoplate under compression. Figure 4(a) shows the normalized minimum eigenvalue η_1^* as a function of compression σ_{app}. Here, the minimum eigenvalue η_1 is normalized according to its magnitude at zero mechanical field, η_1^0. The minimum eigenvalue η_1^0 is positive at $\sigma_{app} = 0$ GPa, indicating that the system is stable. η_1^* is almost a constant at the beginning of the decrease process and then decreases with the decrease of the applied stress. η_1^* reaches zero at point H-I as $\sigma_{app} = -3.2$ GPa and then increases abruptly to a value of about 0.5. It should be noted that the stress magnitude at point H-I with $\eta_1^* = 0$, which indicates the onset of instability, agrees exactly with the respective mechanical field for the initiation of transformation from single- to triple-vortex states, as described in Figs. 3(a) and 3(b). Similarly, in the increase process of the mechanical load, the normalized minimum eigenvalue η_1^* reaches a zero value at point H-II, where $\sigma_{app} = -0.8$ GPa. Figure 4(b) illustrates the eigenvector distribution that corresponds to $\eta_1^* = 0$ at point H-II, which indicates the instability mode, i.e., the change of polarization with the transformation of triple- to single-vortex states. The instability mode vector is significantly large at the domain walls and the middle area of the nanoplate, while it is relatively small in the other areas, for example, the regions near the top and bottom vortices. This result demonstrates that polarizations at the domain walls and the middle area of the HFE nanoplate are quite sensitive to the change of applied mechanical load. The instability mode vector also demonstrates that the vortices near the top and bottom surfaces are more stable than those in the middle of the HFE

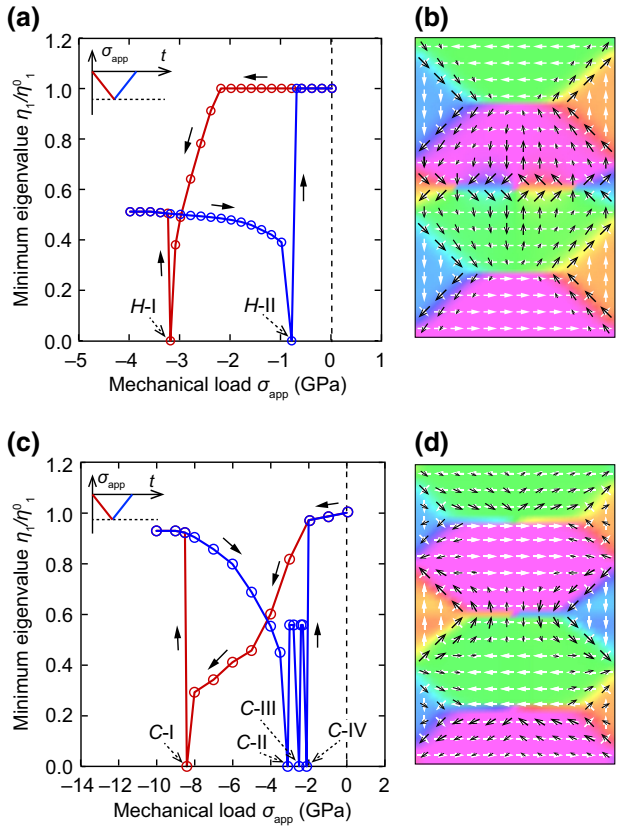

FIG. 4. Minimum eigenvalue as a function of the imposed compression in the first loading-unloading process in (a) HFE and (c) CGFE nanoplates, respectively, with distributions of instability mode vectors corresponding to the zero minimum eigenvalues at points H-II and C-II in (b) HFE and (d) CGFE nanoplates, respectively.

nanoplate. In addition, the instability mode vector clearly shows the changing tendency of the polarization vectors, which corresponds to the onset of polarization transformation from triple- to single-vortex states in the unloading process. The obtained results shown in Figs. 4(a) and 4(b) not only confirm when the polarization switching in a HFE nanoplate occurs, but also demonstrates how the polarization responds at the onset of the switching.

For the CGFE nanoplate, the normalized minimum eigenvalue η_1^* is shown in Fig. 4(c) as a function of the imposed compression. In the first decrease process of compression, the system is stable at $\sigma_{app} = 0$ GPa as the minimum eigenvalue η_1^0 is positive. Then, η_1^* decreases in value as σ_{app} decreases and reaches a zero value at $\sigma_{app} = -8.2$ GPa (point C-I), where the transformation from single- to triple-vortex states occurs. In the increase process of compression, there are three positions where η_1^* drops to zero (from C-II to C-IV), which correspond to the successive transitions from triple- to single-vortex states through several metastable states in a CGFE nanoplate. Figure 4(d) illustrates the instability mode vector, which corresponds to $\eta_1^* = 0$ at $\sigma_{app} = -3.6$ GPa [point C-II in Fig. 4(c)] in the increase process. The instability mode vector is dominant at the domain walls and vortex cores near the top and bottom surfaces, while it is relatively small in the other areas. A similar distribution of the instability mode vectors can be obtained for $\eta_1^* = 0$ at points C-III and C-IV. This result demonstrates that the motions of domain walls and vortex cores near the top and bottom surfaces are the most favorable instability phenomenon that occurs in the CGFE nanoplate under mechanical load. In other words, the CW vortex in the middle of the CGFE nanoplate is likely to remain during the polarization change in the unloading process. Therefore, the instability analyses clearly show the underlying mechanism of stress-induced vortex switching in the CGFE nanoplate.

We further consider the distributions of total and coupling energy densities in HFE and CGFE nanoplates that correspond to points H-II and C-II shown in Figs. 4(a) and 4(c), respectively. In a HFE nanoplate [Figs. 5(a) and 5(b)], the total and coupling energy densities highly concentrate at the domain walls and vortex cores. Since vortex cores near the top and bottom surfaces are surrounded by small magnitudes of total and coupling energy densities, these vortices are less sensitive to the applied stress and become relatively more stable than the middle vortex. Particularly, both total and coupling energy densities highly concentrate near the vortex core at the middle of the nanoplate. Therefore, the middle vortex is likely to be annihilated, which is consistent with the instability mode

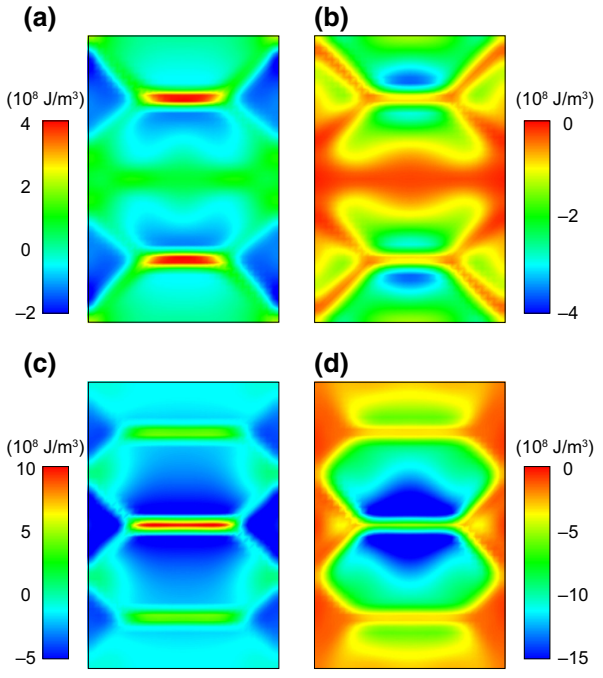

FIG. 5. Distributions of (a) total and (b) electromechanical coupling energy densities in a HFE nanoplate and distributions of (c) total and (d) electromechanical coupling energy densities in a CGFE nanoplate.

and switching phenomenon in the HFE nanoplate. On the other hand, in the CGFE nanoplate [Figs. 5(c) and 5(d)], the total and coupling energy densities also highly concentrate at the domain walls and vortex cores. However, in the area surrounding the vortex core in the middle of the nanoplate, both total and coupling energy densities are relatively small, which tends to preserve this vortex during the evolution. In contrast, the total and coupling energy densities highly concentrate near the top and bottom surfaces, such that the polarization in these areas is likely to be switched during the evolution and, thereby, two vortices near the top and bottom surfaces are cleared away.

D. Effects of various factors on the switching of polarization vortex: Material gradient, temperature, and geometry of CGFE nanoplate

To provide a comprehensive viewpoint on the feasibility of stress-induced switching of polarization vortices in a CGFE nanoplate, the effects of several factors are investigated. At first glance, there should exist a suitable material gradient beyond which the switching of a polarization vortex is prohibited. When the gradient of material compositions is small enough, its effect should be small and the switching behavior is similar to that in HFE (type A). An increase of material gradient could enhance the stability of the vortex at the area with a high mole fraction of PT and lead to more feasible switching (type B). However, when the material gradient is large enough, the evolution path of vortex switching is expected to be different. To make this point clear, we fix the material composition at the middle of the nanoplate as PT, while the material compositions at the top and bottom surfaces are simultaneously changed. Note that the constituent materials vary linearly from the middle of the nanoplate to the top and bottom surfaces.

Snapshots of the vortex evolution for three CGFE nanoplates with different material gradients, i.e., PST10⇔PT⇔PST10, PST20⇔PT⇔PST20, and PST40⇔PT⇔PST40, near room temperature (300 K) are shown in Figs. 6(a)–6(c), respectively. It can be seen that a CGFE nanoplate with the material gradient being PST10⇔PT⇔PST10 exhibits domain evolution following type A. However, a CGFE nanoplate with the material gradient being PST40⇔PT⇔PST40 exhibits a different domain evolution. More specifically, in the loading process, the initial CCW single vortex is switched to triple vortices. However, the triple-vortex state has alternative CW-CCW-CW vorticities, which is opposite to that in the CGFE nanoplate of PST20⇔PT⇔PST20. In the unloading process, the middle vortex with CCW vorticity clears away the other vortices. After the loading-unloading process, the CCW vorticity of single vortex still preserves. Therefore, the switching of a polarization vortex in the CGFE nanoplate of PST40⇔PT⇔PST40 is prohibited. This switching behavior is regarded as type C.

We further conduct simulations for CGFE nanoplate with various material gradients under different temperature conditions. Figure 6(d) depicts a phase diagram, which summarizes the feasibility of stress-induced vortex switching in CGFE nanoplates with various material gradients under different temperature conditions. Near room temperature (300 K), the polarization vortex can be switched by mechanical load in CGFE nanoplates as the material gradient changes in a range from PST16⇔PT⇔PST16 to PST30⇔PT⇔PST30. In addition, one can see from Fig. 6(d) that the range of the material gradient for the switching of a single vortex increases with the decrease of temperature.

Finally, the effect of the width-to-height ratio of a CGFE nanoplate on the feasibility of stress-induced vortex switching is considered. In the investigation of this section, we keep the lateral size of a CGFE nanoplate to be $w \times h \approx 384$ nm^2, but change the width-to-height ratio w/h of CGFE nanoplates from 0.5 to 1.0. The material composition of a CGFE nanoplate is selected as PST20⇔PT⇔PST20. From the preliminary results, we also observe three types of vortex switching, e.g., types A, B, and C, as discussed in previous sections. Figure 6(e) shows a phase diagram that summarizes the feasibility of stress-induced vortex switching in CGFE nanoplates with various w/h ratios under different temperature conditions. Near room temperature (300 K), the polarization vortex can be switched as w/h in a range of [0.6, 0.85]. The range of the w/h ratio for vortex switching increases with the increase of temperature.

On the other hand, inhomogeneous distributions of strain and polarization magnitudes in the CGFE nanoplate exhibit steep gradients in strain and polarization fields [Fig. 2(b)] that lead to flexoelectricity. The flexoelectric effect contributes to enhance the electromechanical coupling [55]. Since the coupling between polarization and strain is one of the sources for the vortex switching, the flexoelectricity may affect the magnitude of applied stress at which the vortex switching occurs, while the switching behavior of a polarization vortex in a CGFE nanoplate may not change in general. However, a quantitative consideration for the influence of the flexoelectric effect on the stress-induced switching of a polarization vortex is kept for future work.

It should be noted that the mechanical stress and strain can be imparted into a nanoplate through a lattice parameter mismatch and differences in thermal expansion behavior between the nanoplate and the underlying substrate or they can arise from grain boundaries and defects formed during fabrication [56–58]. However, exerting a well-controlled stress (or strain) on a nanoplate in practice requires some techniques. There are several practical methods being employed. One possible approach is using the tip of an atomic force microscope pushed onto the surface of a nanoplate; thus, a compressive stress can be induced

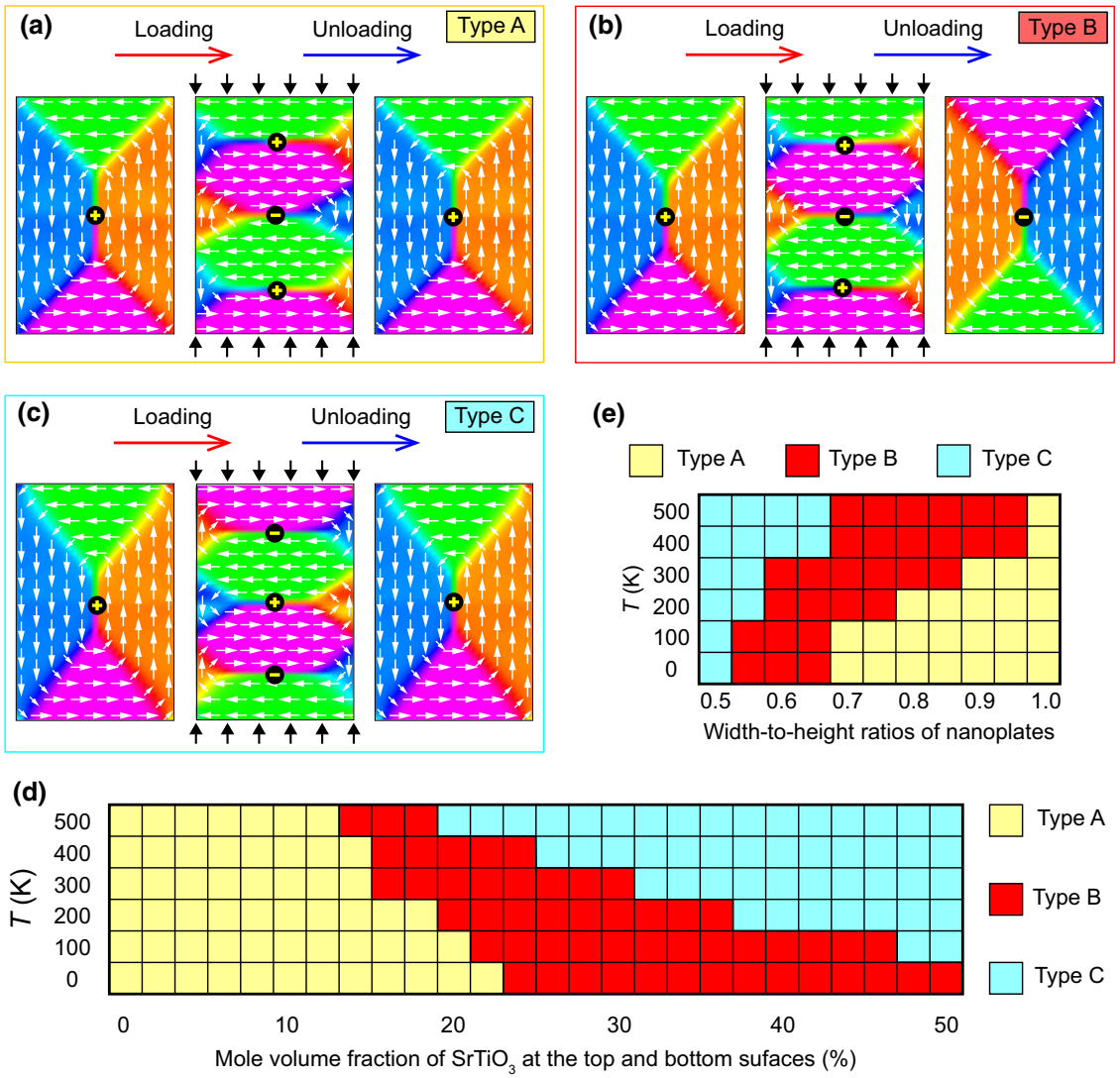

FIG. 6. Snapshots of the vortex evolution for three CGFE nanoplates with different material gradients: (a) PST10⇔PT⇔PST10, (b) PST20⇔PT⇔PST20, and (c) PST40⇔PT⇔PST40, near room temperature (300 K). (d) Phase diagram summarizing the feasibility of vortex switching in CGFE nanoplates with various material gradients and temperature conditions. (e) Phase diagram summarizing the feasibility of vortex switching in CGFE nanoplates with different width-to-height ratios and temperature conditions.

due to the tip [59–61]. Another approach is the use of magnetic-ferroelectric composites, where a large strain can be induced and controlled in the magnetic phase by an external magnetic field due to the magnetostrictive effect. This strain transfers to the ferroelectric phase through interfaces between magnetic and ferroelectric phases [62–64]. In addition, a designed bending device is also a usable tool providing good control over stress (or strain) on nanoplates [65].

IV. CONCLUSIONS

In this work, the formation and transformation of a polarization vortex in a CGFE nanoplate under mechanical excitations is systematically investigated. It is found that stabilization of a single-vortex state is enhanced in CGFE nanoplates and the switching of a polarization vortex under mechanical compression becomes feasible. The rational distribution of material constituents in CGFE nanoplates can tailor the distributions of electromechanical coupling and total energy densities in the nanoplate and, consequently, the stress-induced vortex multiplication and annihilation behavior is modified. The switching of a polarization vortex by mechanical compression is further verified by instability analyses, which not only confirm when the polarization switching in a CGFE nanoplate occurs, but also demonstrates how the polarization responds at the onset of the switching. Furthermore, we systematically discuss the effects of various factors on the feasibility of stress-induced vortex

switching, including the material gradient, temperature, and width-to-height ratio of the CGFE nanoplate.

ACKNOWLEDGMENTS

This research is funded by the Vietnam National Foundation for Science and Technology Development (NAFOSTED) under Grant No. 103.02-2018.06.

[1] I. I. Naumov, L. Bellaiche, and H. Fu, Unusual phase transitions in ferroelectric nanodisks and nanorods, Nature **432**, 737 (2004).

[2] S. Prosandeev and L. Bellaiche, Characteristics and signatures of dipole vortices in ferroelectric nanodots: First-principles-based simulations and analytical expressions, Phys. Rev. B **75**, 094102 (2007).

[3] I. Naumov and H. Fu, Vortex-to-polarization Phase Transformation Path in Ferroelectric $Pb(ZrTi)O_3$ Nanoparticles, Phys. Rev. Lett. **98**, 077603 (2007).

[4] I. Naumov and A. M. Bratkovsky, Unusual Polarization Patterns in Flat Epitaxial Ferroelectric Nanoparticles, Phys. Rev. Lett. **101**, 107601 (2008).

[5] L. Hong, A. K. Soh, S. Y. Liu, and L. Lu, Vortex structure transformation of $BaTiO_3$ nanoparticles through the gradient function, J. Appl. Phys. **106**, 024111 (2009).

[6] K. C. Pitike, J. Mangeri, H. Whitelock, T. Patel, P. Dyer, S. P. Alpay, and S. Nakhmanson, Metastable vortex-like polarization textures in ferroelectric nanoparticles of different shapes and sizes, J. Appl. Phys. **124**, 064104 (2018).

[7] Y. L. Tang, Y. L. Zhu, X. L. Ma, A. Y. Borisevich, A. N. Morozovska, E. A. Eliseev, W. Y. Wang, Y. J. Wang, Y. B. Xu, Z. D. Zhang, and S. J. Pennycook, Observation of a periodic array of flux-closure quadrants in strained ferroelectric $PbTiO_3$ films, Science **348**, 547 (2015).

[8] A. K. Yadav, C. T. Nelson, S. L. Hsu, Z. Hong, J. D. Clarkson, C. M. Schlepütz, A. R. Damodaran, P. Shafer, E. Arenholz, L. R. Dedon, D. Chen, A. Vishwanath, A. M. Minor, L. Q. Chen, J. F. Scott, L. W. Martin, and R. Ramesh, Observation of polar vortices in oxide superlattices, Nature **530**, 198 (2016).

[9] C. M. Dudhe, S. J. Khambadkar, and N. V. Dhoke, Toroidal ferroelectricity in perovskite nanoparticles, Scripta Mater. **131**, 89 (2017).

[10] D. Karpov, Z. Liu, T. dos Santos Rolo, R. Harder, P. Balachandran, D. Xue, T. Lookman, and E. Fohtung, Three-dimensional imaging of vortex structure in a ferroelectric nanoparticle driven by an electric field, Nat. Commun. **8**, 280 (2017).

[11] N. Balke, B. Winchester, W. Ren, Y. H. Chu, A. N. Morozovska, E. A. Eliseev, M. Huijben, R. K. Vasudevan, P. Maksymovych, J. Britson, S. Jesse, I. Kornev, R. Ramesh, L. Bellaiche, L. Q. Chen, and S. V. Kalinin, Enhanced electric conductivity at ferroelectric vortex cores in $BiFeO_3$, Nat. Phys. **8**, 81 (2012).

[12] I. I. Naumov and H. Fu, Cooperative Response of $Pb(ZrTi)O_3$ Nanoparticles to Curled Electric Fields, Phys. Rev. Lett. **101**, 197601 (2008).

[13] J. Wang, Switching mechanism of polarization vortex in single-crystal ferroelectric nanodots, Appl. Phys. Lett. **97**, 192901 (2010).

[14] L. V. Lich, T. Shimada, J. Wang, and T. Kitamura, Instability criterion for ferroelectrics undermechanical/electric multi-fields: Ginzburg-landau theory based modeling, Acta Mater. **112**, 1 (2016).

[15] S. Prosandeev, I. Ponomareva, I. Kornev, I. Naumov, and L. Bellaiche, Controlling Toroidal Moment by Means of an Inhomogeneous Static Field: An Ab Initio Study, Phys. Rev. Lett. **96**, 237601 (2006).

[16] S. Prosandeev, I. Ponomareva, I. Kornev, and L. Bellaiche, Control of Vortices by Homogeneous Fields in Asymmetric Ferroelectric and Ferromagnetic Rings, Phys. Rev. Lett. **100**, 047201 (2008).

[17] W. J. Chen, Y. Zheng, B. Wang, and J. Y. Liu, Coexistence of toroidal and polar domains in ferroelectric systems: A strategy for switching ferroelectric vortex, J. Appl. Phys. **115**, 214106 (2014).

[18] L. VanLich, T. Shimada, J. Wang, V.-H. Dinh, T. Q. Bui, and T. Kitamura, Switching the chirality of a ferroelectric vortex in designed nanostructures by a homogeneous electric field, Phys. Rev. B **96**, 134119 (2017).

[19] W. J. Chen and Y. Zheng, Vortex switching in ferroelectric nanodots and its feasibility by a homogeneous electric field: Effects of substrate, dislocations and local clamping force, Acta Mater. **88**, 41 (2015).

[20] X. Ren, Large electric-field-induced strain in ferroelectric crystals by point-defect-mediated reversible domain switching, Nat. Mater. **3**, 91 (2004).

[21] J. F. Scott and C. A. P. De Araujo, Ferroelectric memories, Science **246**, 1400 (1989).

[22] C.-P. De Araujo, J. D. Cuchiaro, L. D. McMillan, M. C. Scott, and J. F. Scott, Fatigue-free ferroelectric capacitors with platinum electrodes, Nature **374**, 627 (1995).

[23] J. F. Scott and M. Dawber, Oxygen-vacancy ordering as a fatigue mechanism in perovskite ferroelectrics, Appl. Phys. Lett. **76**, 3801 (2000).

[24] W. J. Chen, Y. Zheng, and B. Wang, Vortex domain structure in ferroelectric nanoplatelets and control of its transformation by mechanical load, Sci. Rep. **2**, 796 (2012).

[25] W. J. Chen, Y. Zheng, and B. Wang, Phase field simulations of stress controlling the vortex domain structures in ferroelectric nanosheets, Appl. Phys. Lett. **100**, 062901 (2012).

[26] L. V. Lich, T. Shimada, K. Nagano, Y. Hongjun, J. Wang, K. Huang, and T. Kitamura, Anomalous toughening in nanoscale ferroelectrics with polarization vortices, Acta Mater. **88**, 147 (2015).

[27] S. Yuan, W. J. Chen, L. L. Ma, Y. Ji, W. M. Xiong, J. Y. Liu, Y. L. Liu, B. Wang, and Y. Zheng, Defect-mediated vortex multiplication and annihilation in ferroelectrics and the feasibility of vortex switching by stress, Acta Mater. **148**, 330 (2018).

[28] N. D. Mermin, The topological theory of defects in ordered media, Rev. Mod. Phys. **51**, 591 (1979).

[29] L. V. Lich, T. Shimada, J. Wang, and T. Kitamura, Self-ordering of nontrivial topological polarization structures in nanoporous ferroelectrics, Nanoscale **9**, 15525 (2017).

[30] L. V. Lich, Q.-T. Ton, T.-G. Nguyen, and V.-H. Dinh, On the correlation between topological defects of polarization field and Euler characteristics of ferroelectric nanostructures, Appl. Phys. Lett. **114**, 022901 (2019).
[31] S. Prosandeev, A. Malashevich, Z. Gui, A. Malashevich, L. Louis, R. Walter, I. Souza, and L. Bellaiche, Natural optical activity and its control by electric field in electrotoroidic systems, Phys. Rev. B **87**, 195111 (2013).
[32] B. Winchester, N. Balke, X. X. Cheng, A. N. Morozovska, S. Kalinin, and L. Q. Chen, Electroelastic fields in artificially created vortex cores in epitaxial $BiFeO_3$ thin films, Appl. Phys. Lett. **107**, 052903 (2015).
[33] G. A. Schneider, Influence of electric field and mechanical stresses on the fracture of ferroelectrics, Annu. Rev. Mater. Res. **37**, 491 (2007).
[34] M. Kuna, Fracture mechanics of piezoelectric materials–where are we right now? Eng. Fract. Mech. **77**, 309 (2010).
[35] J. Mangeri, S. P. Alpay, S. Nakhmanson, and O. G. Heinonen, Electromechanical control of polarization vortex ordering in an interacting ferroelectric-dielectric composite dimer, Appl. Phys. Lett. **113**, 092901 (2018).
[36] J. C. Agar, A. R. Damodaran, M. B. Okatan, J. Kacher, C. Gammer, R. K. Vasudevan, S. Pandya, L. R. Dedon, R. V. K. Mangalam, G. A. Velarde, S. Jesse, N. Balke, A. M. Minor, S. V. Kalinin, and L. W. Martin, Highly mobile ferroelastic domain walls in compositionally graded ferroelectric thin films, Nat. Mater. **15**, 549 (2016).
[37] A. R. Damodaran, S. Pandya, Y. Qi, S.-L. Hsu, S. Liu, C. Nelson, A. Dasgupta, P. Ercius, C. Ophus, and L. R. Dedon *et al.*, Large polarization gradients and temperature-stable responses in compositionally-graded ferroelectrics, Nat. Commun. **8**, 14961 (2017).
[38] H.-L. Hu and L.-Q. Chen, Three-dimensional computer simulation of ferroelectric domain formation, J. Am. Ceram. Soc. **81**, 492 (1998).
[39] Y. L. Li, S. Y. Hu, Z. K. Liu, and L. Q. Chen, Phase-field model of domain structures in ferroelectric thin films, Appl. Phys. Lett. **78**, 3878 (2001).
[40] S. Y. Hu and L. Q. Chen, A phase-field model for evolving microstructures with strong elastic inhomogeneity, Acta Mater. **49**, 1879 (2001).
[41] L.-Q. Chen, Phase-field models for microstructure evolution, Ann. Rev. Mater. Res. **32**, 113 (2002).
[42] J. Mangeri, Y. Espinal, A. Jokisaari, S. P. Alpay, S. Nakhmanson, and O. Heinonen, Topological phase transformations and intrinsic size effects in ferroelectric nanoparticles, Nanoscale **9**, 1616 (2017).
[43] G. Zhang, X. Zhang, T. Yang, Q. Li, L.-Q. Chen, S. Jiang, and Q. Wang, Colossal room-temperature electrocaloric effect in ferroelectric polymer nanocomposites using nanostructured barium strontium titanates, ACS Nano **9**, 7164 (2015).
[44] I. B. Misirlioglu and S. P. Alpay, Compositionally graded ferroelectrics as wide band gap semiconductors: Electrical domain structures and the origin of low dielectric loss, Acta Mater. **122**, 266 (2017).
[45] L. V. Lich, T. Shimada, S. Sepideh, J. Wang, and T. Kitamura, Multilevel hysteresis loop engineered with ferroelectric nano-metamaterials, Acta Mater. **125**, 202 (2017).
[46] L. V. Lich and V.-H. Dinh, Formation of polarization needle-like domain and its unusual switching in compositionally graded ferroelectric thin films: An improved phase field model, RSC Adv. **9**, 7575 (2019).
[47] T. Kitamura, Y. Umeno, and N. Tsuji, Analytical evaluation of unstable deformation criterion of atomic structure and its application to nanostructure, Comput. Mater. Sci. **29**, 499 (2004).
[48] T. Kitamura, Y. Umeno, and R. Fushino, Instability criterion of inhomogeneous atomic system, Mater. Sci. Eng. A **379**, 229 (2004).
[49] T. Shimada, S. Okawa, S. Minami, and T. Kitamura, Simplified evaluation of mechanical instability in large-scale atomic structures, Mater. Sci. Eng. A **513**, 166 (2009).
[50] T. Shimada, K. Ouchi, I. Ikeda, Y. Ishii, and T. Kitamura, Magnetic instability criterion for spin–lattice systems, Comput. Mater. Sci. **97**, 216 (2015).
[51] A. R. Balakrishna and J. E. Huber, Scale effects and the formation of polarization vortices in tetragonal ferroelectrics, Appl. Phys. Lett. **106**, 092906 (2015).
[52] Y. L. Li, S. Choudhury, J. H. Haeni, M. D. Biegalski, A. Vasudevarao, A. Sharan, H. Z. Ma, J. Levy, V. Gopalan, S. Trolier-McKinstry, D. G. Schlom, Q. X. Jia, and L. Q. Chen, Phase transitions and domain structures in strained pseudocubic (100) $SrTiO_3$ thin films, Phys. Rev. B **73**, 184112 (2006).
[53] G. Sheng, Y. L. Li, J. X. Zhang, S. Choudhury, Q. X. Jia, V. Gopalan, D. G. Schlom, Z. K. Liu, and L. Q. Chen, Phase transitions and domain stabilities in biaxially strained (001) $SrTiO_3$ epitaxial thin films, J. Appl. Phys. **108**, 084113 (2010).
[54] Y. C. Song, Y. Ni, and J. Q. Zhang, Phase field model of polarization evolution in a finite ferroelectric body with free surfaces, Acta Mech. **224**, 1309 (2013).
[55] P. Zubko, G. Catalan, and A. K. Tagantsev, Flexoelectric effect in solids, Annu. Rev. Mater. Res. **43**, 387 (2013).
[56] L. B. Freund and S. Suresh, *Thin Film Materials: Stress, Defect Formation and Surface Evolution* (Cambridge University Press, 2004).
[57] W. D. Nix and B. M. Clemens, Crystallite coalescence: A mechanism for intrinsic tensile stresses in thin films, J. Mater. Res. **14**, 3467 (1999).
[58] T. R. Taylor, P. J. Hansen, B. Acikel, N. Pervez, R. A. York, S. K. Streiffer, and J. S. Speck, Impact of thermal strain on the dielectric constant of sputtered barium strontium titanate thin films, Appl. Phys. Lett. **80**, 1978 (2002).
[59] H. Lu, C.-W. Bark, D. E. De Los Ojos, J. Alcala, C.-B. Eom, G. Catalan, and A. Gruverman, Mechanical writing of ferroelectric polarization, Science **336**, 59 (2012).
[60] P. Gao, J. Britson, C. T. Nelson, J. R. Jokisaari, C. Duan, M. Trassin, S.-H. Baek, H. Guo, L. Li, Y. Wang, Y.-H. Chu, A. M. Minor, C.-B. Eom, R. Ramesh, L.-Q. Chen, and X. Pan, Ferroelastic domain switching dynamics under electrical and mechanical excitations, Nat. Commun. **5**, 3801 (2014).
[61] Z. Chen, L. Hong, F. Wang, X. An, X. Wang, S. Ringer, L.-Q. Chen, H. Luo, and X. Liao, Kinetics of Domain Switching by Mechanical and Electrical Stimulation in

Relaxor-based Ferroelectrics, Phys. Rev. Appl. **8**, 064005 (2017).

[62] K. C. Verma, M. Singh, R. K. Kotnala, and N. Goyal, Magnetic field control ofpolarization/capacitance/voltage/resistance through lattice strain in $BaTiO_3$-$CoFe_2O_4$ multiferroic nanocomposite, J. Magn. Magn. Mater. **469**, 483 (2019).

[63] L. V. Lich, T. Shimada, K. Miyata, K. Nagano, J. Wang, and T. Kitamura, Colossal magnetoelectric effect in 3-1 multiferroic nanocomposites originating from ultrafine nanodomain structures, Appl. Phys. Lett. **107**, 232904 (2015).

[64] S. Poddar, P. de Sa, R. Cai, L. Delannay, B. Nysten, L. Piraux, and A. M. Jonas, Room-temperature magnetic switching of the electric polarization in ferroelectric nanopillars, ACS Nano **12**, 576 (2018).

[65] H.-M. Yau, Z. Xi, X. Chen, Z. Wen, G. Wu, and J.-Y. Dai, Dynamicstrain-induced giant electroresistance and erasing effect in ultrathin ferroelectric tunnel-junction memory, Phys. Rev. B **95**, 214304 (2017).